Chemistry
A European
Journal

Chemistry Europe
European Chemical Societies Publishing

## Accepted Article

**Title:** Interaction of Hydrogen with Ceria: Hydroxylation, Reduction, and Hydride Formation on the Surface and in the Bulk

**Authors:** Zhaorui Li, Kristin Werner, Lu Chen, Aiping Jia, Kun Qian, Jian-Qiang Zhong, Rui You, Lihui Wu, Liyuan Zhang, Haibin Pan, Xin Ping Wu, Xue-Qing Gong, Shamil Shaikhutdinov, Weixin Huang, and Hans-Joachim Freund



**To be cited as:** *Chem. Eur. J.* 10.1002/chem.202005374

**Link to VoR:** https://doi.org/10.1002/chem.202005374

WILEY-VCH

10.1002/chem.202005374

# Interaction of Hydrogen with Ceria: Hydroxylation, Reduction, and Hydride Formation on the Surface and in the Bulk

Zhaorui Li,[1#] Kristin Werner,[2#] Lu Chen,[3#] Aiping Jia,[1,4] Kun Qian,[1] Jian-Qiang Zhong,[2] Rui You,[1] Lihui Wu,[5] Liyuan Zhang,[1] Haibin Pan,[5] Xin-Ping Wu,[3]* Xue-Qing Gong,[3] Shamil Shaikhutdinov[2]*, Weixin Huang,[1,6]* Hans-Joachim Freund[2]

[1] Hefei National Laboratory for Physical Sciences at Microscale, Key Laboratory of Surface and Interface Chemistry and Energy Catalysis of Anhui Higher Education Institutes, CAS Key Laboratory of Materials for Energy Conversion and Department of Chemical Physics, University of Science and Technology of China, Hefei 230026, P. R. China
[2] Fritz-Haber-Institut der Max-Planck Gesellschaft, Faradayweg 4-6, Berlin 14195, Germany
[3] Key Laboratory for Advanced Materials and Joint International Research Laboratory for Precision Chemistry and Molecular Engineering, Feringa Nobel Prize Scientist Joint Research Center, Centre for Computational Chemistry and Research Institute of Industrial Catalysis, School of Chemistry and Molecular Engineering, East China University of Science and Technology, 130 Meilong Road, Shanghai, 200237, P.R. China.
[4] Key Laboratory of the Ministry of Education for Advanced Catalysis Materials, Institute of Physical Chemistry, Zhejiang Normal University, Jinhua 321004, P. R. China
[5] National Synchrotron Radiation Laboratory, University of Science and Technology of China, Hefei 230029, P. R. China
[6] Dalian National Laboratory for Clean Energy, Dalian 116023, P. R. China

[#]These authors contributed equally.

*Corresponding authors. E-mail addresses: huangwx@ustc.edu.cn (Weixin Huang), shaikhutdinov@fhi-berlin.mpg.de (Shamil Shaikhutdinov), xpwu@ecust.edu.cn (Xin-Ping Wu)

**Abstract.** The study reports on a first attempt to address the interplay between surface and bulk in hydride formation in ceria ($CeO_2$) by combining experiment, using surface sensitive and bulk sensitive spectroscopic techniques on the two sample systems, *i.e.*, $CeO_2$(111) thin films and $CeO_2$ powders, and theoretical calculations of $CeO_2$(111) surfaces with oxygen vacancies ($O_v$) at the surface and in the bulk. We show that, on a stoichiometric $CeO_2$(111) surface, $H_2$ dissociates and forms surface hydroxyls (OH). On the pre-reduced $CeO_{2-x}$ samples, both films and powders, hydroxyls and hydrides (Ce-H) are formed on the surface as well as in the bulk, accompanied by the $Ce^{3+}\leftrightarrow Ce^{4+}$ redox reaction. As the $O_v$ concentration increases, hydroxyl is destabilized and hydride becomes more stable. Surface hydroxyl is more stable than bulk hydroxyl, whereas bulk hydride is more stable than surface hydride. The surface hydride formation is the kinetically-favorable process at relatively low temperatures, and the resulting surface hydride may diffuse into the bulk region and be stabilized therein. At higher temperatures, surface hydroxyls can react to produce water and create additional oxygen vacancies, increasing its concentration, which controls the $H_2/CeO_2$ interaction. The results demonstrate a large diversity of reaction pathways, which have to be taken into account for better understanding of reactivity of ceria-based catalysts in a hydrogen-rich atmosphere.

**Keywords:** Ceria; Hydride; Hydrogenation; Surface structure; Density functional theory

10.1002/chem.202005374

## 1. Introduction

Interaction of hydrogen with metal oxides is intimately involved in many important processes, from $H_2$ storage to thermal, photo- and electro-catalysis.[1] It exhibits complex behavior,[2] including homolytic dissociation at two oxygen sites, thermodynamically favored for readily reducible oxides leading to two hydroxyl (OH) groups and the concomitant reduction of two surface metal cations, and heterolytic dissociation at metal and oxygen sites primarily occurring on oxides difficult to reduce. The process may involve the migration of H atoms into the sub-surface region and the bulk to form hydroxyl and hydride ($H^-$) species therein.

Beyond this, the interaction of $H_2$ with ceria ($CeO_2$) has recently received great attention because ceria, widely used as oxidation catalysts, demonstrate the potential as a selective catalyst for alkyne semi-hydrogenation reactions.[3] It is assumed that $H_2$ undergoes dissociation forming two surface OH groups.[4] The resulting OHs react to produce water at elevated temperatures, creating oxygen vacancies ($O_v$). Density functional theory (DFT) calculations showed that the homolytic dissociation of $H_2$ at two oxygen sites is thermodynamically favored on fully oxidized, stoichiometric $CeO_2$(111) surface.[5] However, the calculations also suggested a heterolytic $H_2$ dissociation to be kinetically favored on this surface to form a Ce-H and a OH species.[6] The resulting Ce-H species further evolve to the thermodynamically more stable OH species, accompanied by the reduction of $Ce^{4+}$ into $Ce^{3+}$.

Oxygen vacancies on a ceria surface have been shown, both theoretically and experimentally, to strongly affect the $H_2$-$CeO_2$ interaction. The oxygen vacancies can even be formed *in situ* during the reaction, *e.g.*, by desorption of water *via* recombination of surface OHs. Theoretical calculations indicated that the stability of Ce-H species resulting from heterolytic $H_2$ dissociation is enhanced on reduced, *i.e.,* $O_v$-containing ceria surfaces.[7] Experimentally, surface oxygen vacancies on $CeO_2$ were observed to affect the reactivity of surface hydroxyls by suppressing the water production pathway and promoting the $H_2$ production pathway.[8] In addition, the processes may be influenced by oxygen vacancy diffusion, as water formation and the accompanied oxygen vacancy formation happens on the surface. According to DFT calculations,[9] both, vacancy formation and diffusion, are rather independent of surface orientation. Using inelastic neutron scattering spectroscopy, Wu *et al.* [10] first reported the direct spectroscopic evidence for the formation of Ce-H species upon $H_2$ dissociation over ceria powder naturally containing oxygen vacancies. Werner *et al.*[11]

10.1002/chem.202005374

observed that $H_2$ dissociation on a fully oxidized $CeO_2$(111) thin film surface forms hydroxyl species, primarily located at the surface, while on the reduced $CeO_{2-x}$(111) thin films Ce-H species were also found in appreciable quantities below the surface indicating that the absorption of hydrogen leads to the formation of $O_v$-stabilized hydride species in the bulk. Furthermore, $H_2$ adsorption at room temperature was shown to lead to the oxidation of $Ce^{3+}$ in both $CeO_{2-x}$(111) thin films and $CeO_{2-x}$ powders to $Ce^{4+}$,[12] demonstrating the formation of more Ce-H hydride species at the $Ce^{3+}$-$O_v$ sites than OH species at the O sites. Very recently, Schweke *et al.*[13] using thermal gravimetric analysis and thermal desorption spectroscopy of ceria powders studied the influence of temperature, hydrogen partial pressure, and oxygen vacancies on the $H_2$-$CeO_2$ interaction. The presence of oxygen vacancies was found to lead to the penetration of hydrogen into the sub-surface and bulk, possibly as hydride species.

The likely net chemical reactions between $H_2$ and ceria include:

Homolytic dissociation to OH: $H_2(g) + 2Ce^{4+} + 2O^{2-} \rightarrow 2OH^- + 2Ce^{3+}$ (1)

Oxygen vacancy formation: $H_2(g) + 2Ce^{4+} + O^{2-} \rightarrow H_2O(g) + 2Ce_{Ov}^{3+}$ (2)

Homolytic dissociation to Ce-H: $H_2(g) + 2Ce_{Ov}^{3+} \rightarrow 2Ce_{Ov}^{4+}H^-$ (3)

Heterolytic dissociation: $H_2(g) + Ce^{4+} + O^{2-} \rightarrow OH^- + Ce^{4+}H^-$ (4)

It is obvious that the $H_2$-$CeO_2$ interaction is complex and quite sensitive to the reaction conditions. Combined studies on model systems with different levels of complexity have been demonstrated to be an effective strategy towards a fundamental understanding of complex systems.[14] Herein, we report a comprehensive experimental study of $H_2$ interaction with well-defined $CeO_2$(111) thin films and $CeO_2$ powders in wide range of temperatures and pressures, combined with DFT calculations of $CeO_2$(111) surfaces with oxygen vacancies at the surface and in the bulk. We provide spectroscopic evidences for the interplay between hydroxyl and hydride formation within the bulk, and connect those results to the evidence presented for the corresponding species on the surface and in the near surface region, allowing us to reach a consistent picture.

## 2. *Results and discussion*

### *2.1. Ceria thin films*

10.1002/chem.202005374

We first address experimental results obtained on the fully stoichiometric $CeO_2$(111) thin films using Infrared Reflection Absorption Spectroscopy (IRAS) and X-ray Photoelectron Spectroscopy (XPS). Figure 1a shows a series of IRAS spectra measured in 10 mbar of $D_2$ at several temperatures in the range of 300 – 600 K. Basically, no reaction occurs at 300 K. On the sample exposed to $D_2$ at 400 K (henceforth denoted as "$CeO_2$-400"), $D_2$ dissociates forming OD species identified by the $\nu$(OD) band at about 2700 $cm^{-1}$ depending on exposure (see Figure S1 in Supporting Information (SI)). Upon cooling to 235 K in $D_2$ atmosphere, the band increases in intensity and shifts to the higher wavenumbers. Interestingly, this band disappears after pumping $D_2$ out. However, it only decreases in intensity on the "$CeO_2$-500" sample while the intensity remains on the "$CeO_2$-600" sample, thus indicating different stability of surface ODs formed at different adsorption temperatures. Concomitantly, the $\nu$(OH) bands at 3660 and 3665 $cm^{-1}$ and additional bands at 1295 and 1265 $cm^{-1}$ emerge, which are assigned to adventitious adsorption of residual $H_2O$ and $CO_2$ from the vacuum background.

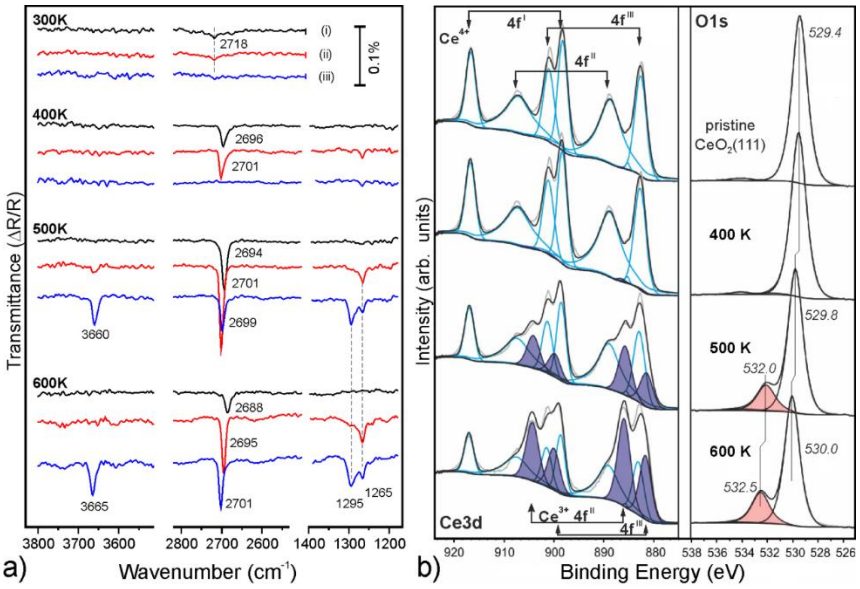


**Figure 1.** a) IRAS spectra measured on a $CeO_2$(111) film in 10 mbar of $D_2$ at the indicated temperature (i); after sample cooling to 235 K (ii); and after subsequent pumping of the $D_2$ gas phase and heating to 300 K (iii). $\nu$(OH), $\nu$(OD), and $\nu_{sym}(CO_2)$ regions are shown. (b) Ce 3d and O 1s XPS spectra measured at grazing emission (60° off-normal) for $CeO_2$(111) films as grown and after $D_2$ exposure at three different temperatures as indicated. The spectral deconvolution is highlighted.

To examine whether the reaction with hydrogen induced changes in the electronic structure, we measured XPS spectra immediately after the IRAS measurements. The spectra

10.1002/chem.202005374

of the Ce3d and O1s core levels were recorded both at normal and grazing emissions, the latter are only shown in Figure 1b. The complex Ce3d spectra in $CeO_2$ are usually rationalized in terms of the spin orbit pairs of the $Ce3d^94f^0O2p^6$, $Ce3d^94f^1O2p^5$ and $Ce3d^94f^2O2p^4$ final states,[15] labeled in the figure as 4f', 4f'' and 4f''', respectively. If present, $Ce^{3+}$ species manifest themselves by additional signals, which correspond to the 4f'' and 4f'''final states. Since the $Ce^{4+}$ and $Ce^{3+}$ states overlap, the degree of ceria reduction can only be determined after a relatively complex deconvolution procedure and background subtraction.

The fully stoichiometric $CeO_2$(111) films exhibited a $Ce^{3+}/(Ce^{3+} + Ce^{4+})$ signal ratio (henceforth, $Ce^{3+}$ concentration) of about 0.01. After reaction with $D_2$ at 300 and 400 K, no additional $Ce^{3+}$ species were detected, suggesting that surface reduction does not occur at low temperatures, in full agreement with the IRAS results. In contrast, considerable amounts of $Ce^{3+}$ are observed after reactions at 500 and 600 K, indicating progressive ceria reduction at high temperatures. A well-resolved O1s signal at the higher binding energy (BE) side of the main peak at 529.4 eV is assigned to OH(OD) and carbonates-like species detected by IRAS (Figure 1a).

It is important to note that, upon increasing the $D_2$ exposure temperature from 500 to 600 K, the intensity of the adsorbates-related O1s signal, normalized to the total O1s signal, only slightly increases, from 0.18 (0.09) to 0.22 (0.1) measured at grazing (normal) emission, whereas the $Ce^{3+}$ concentration measured from analysis of the Ce3d region increases substantially, from 0.28 (0.16) to 0.55 (0.42). This finding indicates that, after the reaction at 600 K, considerable amounts of oxygen vacancies are located not only at the surface (where they would be easily filled by residual water as shown by IRAS), but also in the sub-surface region.

In the next set of experiments, we address interaction of $D_2$ with reduced, *i.e.*, $CeO_{2-x}$(111) film surfaces. Figure 2a summarizes the IRAS results of the exposure experiments at different temperatures. Note that, in contrast to the $CeO_2$(111) surface, the reduced surface may react with traces of water in the UHV background even before the introduction of $D_2$, thus forming OH species as shown in spectra marked by (*) for three different temperatures. The corresponding XPS results are displayed in Figure 2b.

10.1002/chem.202005374

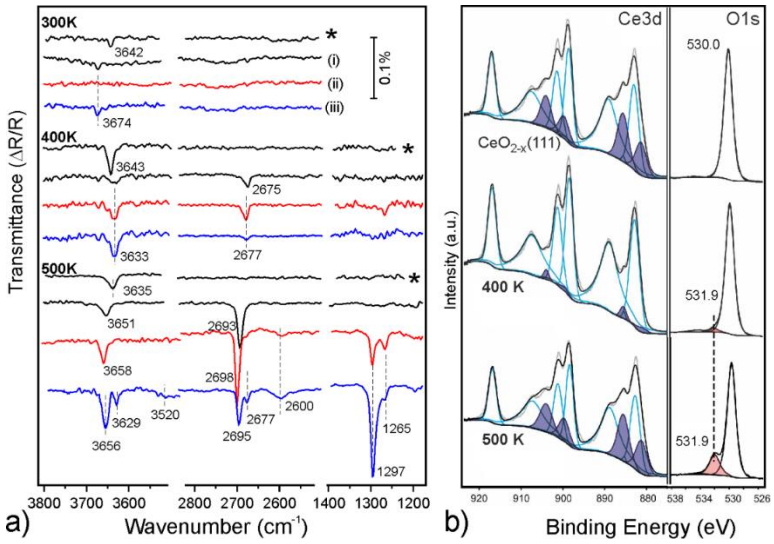


**Figure 2.** a) IRAS spectra recorded on reduced $CeO_{2-x}$(111) films in 10 mbar of $D_2$ at the indicated temperature (i); after sample cooling to 235 K in $D_2$ (ii); and after subsequent pumping out of the $D_2$ gas phase and heating to 300 K (iii). Spectra recorded at 300 K prior to the $D_2$ exposure are marked by (*). b) Ce 3d and O 1s XPS spectra measured at grazing emission (60° off-normal) for reduced $CeO_{2-x}$(111) films as grown and after $D_2$ exposure at two different temperatures indicated. The spectral deconvolution is highlighted.

The results of experiments with $D_2$ at 300 K nicely reproduce our previous results obtained with $H_2$.[12] No surface hydroxyls are observed upon $D_2$ exposure, whereas XPS (not shown here) revealed a strong electronic effect: Almost no $Ce^{3+}$ remain at surface after $D_2$ treatment indicating the formation of $Ce^{4+}$-$D^-$ species.

At 400 K, $D_2$ dissociates giving rise to a weak ν(OD) band at 2675 $cm^{-1}$. Upon cooling in $D_2$, the band gains in intensity together with the OH band (from residual water). After pumping the $D_2$ gas phase out and then heating the sample to 300 K, the OH band increases at the expense of the OD band. However, the measured frequency ratio (ν(OH)/ν(OD) = 1.357) suggests that OH and OD species are identical in nature, thus occupying the same adsorption sites. The interplay between intensities of OH and OD bands can be explained by the H-D exchange reaction and/or by competition between $H_2O$ and $D_2$ for adsorption sites.

Again, after reaction at 400 K, the $Ce^{3+}$ concentration is dramatically decreased (Figure 2b) due to the formation of hydride species. Small amounts of $Ce^{3+}$ originate from surface hydroxyl species, detected by IRAS (Figure 2a) and O1s XPS. Since the integral intensity of the O1s signal remains unchanged after reaction, the observed oxidation of ceria cannot be explained by migration, if any, of lattice O from deeper layers to the surface. Therefore, the interaction of hydrogen with reduced ceria surfaces at 300 and 400 K primarily results in hydride species.

10.1002/chem.202005374

The same experiment at 500 K, however, revealed a different picture. While also here the adsorption of residual $H_2O$ gives rise to a ν(OH) band at 3635 $cm^{-1}$, surface hydroxylation through $D_2$ dissociation dominates the spectra: A strong ν(OD) band appears at 2693 $cm^{-1}$. Upon subsequent cooling and pumping, a weak band emerges around 2600 $cm^{-1}$, which falls in the range of frequencies characteristic for H-bonded hydroxyls,[16] and additional bands appear in both the ν(OH) and ν(OD) regions, *i.e.*, at 3629 and 2677 $cm^{-1}$, respectively. These latter closely resemble those observed in experiments at 400 K, and probably develop during the reaction while sample cooling in $D_2$ atmosphere.

In contrast to the experiments at 300 and 400 K, comparison of the Ce3d spectra before and after reaction with $D_2$ at 500 K revealed similar concentration of $Ce^{3+}$. However, a significant portion of $Ce^{3+}$ species may originate from a high density of surface hydroxyls, which obscure XPS detection of hydride species. It may also well be that H(D) atoms migrate into the deeper layers of ceria at 500 K and thus become "invisible" to surface sensitive XPS. Both the Ce3d and O1s spectra after reaction at 500 K look virtually identical to those obtained during the same experiment on the stoichiometric $CeO_2$(111) film (Figure 1b). Even IRAS spectra measured on $CeO_2$ and $CeO_{2-x}$ films at 500 K in $D_2$ atmosphere display almost identical intensity and position of ν(OD) bands (Figure 3a). Based on these results, one concludes that the initial degree of surface reduction does not play a critical role in the $D_2$-$CeO_2$ interaction at elevated temperatures, since the surface reduction and oxygen vacancy formation occurs *in situ* on the initially oxidized ceria surface *via* recombinative desorption of surface hydroxyls formed by hydrogen dissociation.

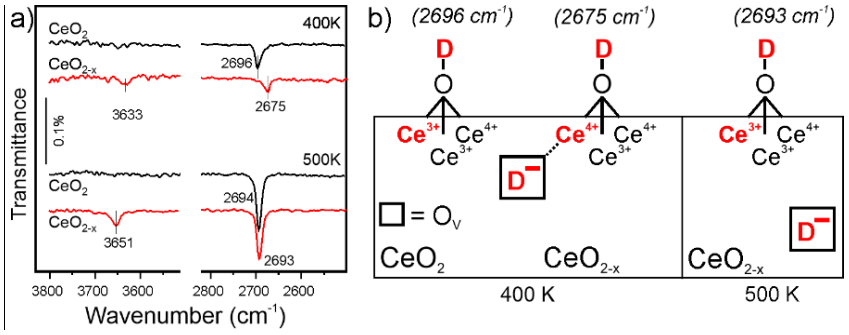


**Figure 3.** (a) Comparison of IRAS spectra measured on $CeO_2$(111) and $CeO_{2-x}$(111) films in 10 mbar of $D_2$ at 400 K and 500 K. (b) Schematic representation of D species formed on oxidized ($CeO_2$) and pre-reduced ($CeO_{2-x}$) surfaces.

10.1002/chem.202005374

It is interesting that the position of the OD bands observed on $CeO_2$ and $CeO_{2-x}$ films at 400 K show considerably different frequencies, *i.e.*, 2696 and 2675 $cm^{-1}$, respectively (see Figure 3a). To rationalize this result, we refer to DFT calculations [11] showing that the frequency depends on the local degree of reduction surrounding the surface hydroxyl, *i.e.*, on the number of $Ce^{3+}$ ions among the three Ce ions the hydroxyl is coordinated to: The more $Ce^{3+}$ ions, the higher the frequency. Therefore, the OD groups formed on the fully oxidized $CeO_2$ surface (2696 $cm^{-1}$) are coordinated to more reduced Ce ions than the OD groups formed on the pre-reduced $CeO_{2-x}$ surface (2675 $cm^{-1}$) (see Figure 3b for a schematic representation). Even though this sounds a bit counterintuitive, the effect can be explained if we recall the XPS results (Figure 2b) showing that the $D_2$ interaction with the reduced $CeO_{2-x}$ surface at 400 K results in hydride species and the oxidation of $Ce^{3+}$ to $Ce^{4+}$. Therefore, the low-frequency band may be assigned to OD which is coordinated to Ce-D hydride species formed on the reduced films (Figure 3b). Such a red-shift could even be used as an indication for hydride species at the surface. In the same manner, the low-frequency "satellite" bands (3629 and 2677 $cm^{-1}$) found for the $CeO_{2-x}$ surface treated at 500 K (Figure 2a) can also be assigned to OH and OD groups on surface hydride sites, which are formed during sample cooling in $D_2$.

Therefore, combined IRAS and XPS study on well-defined $CeO_2$(111) films shows that molecular hydrogen dissociates at relatively high pressures and temperatures and forms surface hydroxyls. On pre-reduced films, however, both surface hydroxyls and hydrides are formed. The hydride formation seems to be the favorable process at relatively low temperatures (< 400 K) within the surface layers probed by XPS, while hydroxylation dominates at higher temperatures, which is accompanied by surface reduction through water desorption.

### *2.2. Ceria powders*

Now we address experimental results for the $H_2$-$CeO_2$ interaction obtained on ceria powders under realistic pressure conditions, *i.e.*, 1 atm 5% $H_2$/He, 1 atm $H_2$, and 10 atm $H_2$, in order to investigate the interplay between surface and bulk in hydroxyl and hydride formation. As shown by electron microscopy (Figure 4), conventional $CeO_2$ powders (from Sigma- Aldrich, see SI) consist of irregularly shaped polyhedral nanoparticles (10 - 50 nm) which primarily expose the (111) facets and minor (110) and (100) facets. [3b,3c,17] This morphology basically

10.1002/chem.202005374

remains after $CeO_2$ powders were treated in 1 atm of $H_2$ at 773 K. Since it has been shown by DFT calculations,[9] that the energies to create oxygen vacancies on the (111), (100) and (110) surfaces are comparable (*i.e.*, 2.0 – 2.6 eV), and all are much smaller than in the bulk (3.4 eV), the comparison between the powder samples and the $CeO_2$(111) thin films appears to be appropriate.

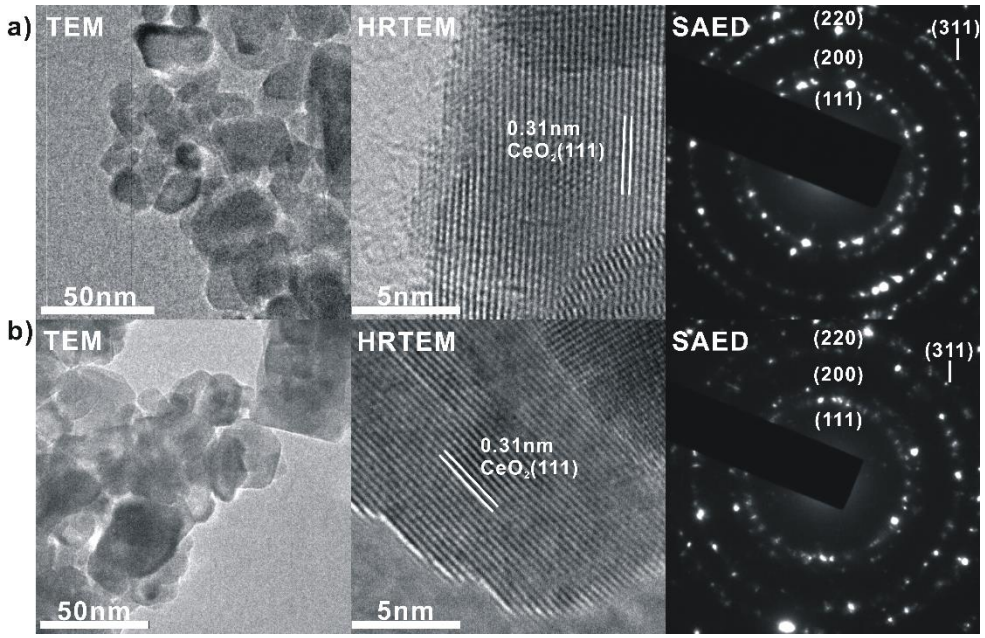


**Figure 4.** TEM and HRTEM images and SAED patterns of ceria powders before (a) and after (b) treatment in 1 atm of $H_2$ at 773 K.

According to the temperature programmed reduction (TPR) spectra (Figure S2), surface reduction in 1 atm of 5% $H_2$/He commences at above 500 K.[8b] In pure $H_2$, the reduction reasonably occurs at lower temperatures (~380 K) and reaches a maximum at 440 K. Hydrogen uptake peak at 615 K is associated with the reduction in sub-surface/bulk region.[8b] Both processes are accompanied by the formation of water. It appears that the reduction of ceria becomes more difficult with increasing $H_2$ pressure to 10 atm. A broad water signal peaked at 522 K may be attributed to reduction both at surface and in sub-surface/bulk layers. Meanwhile, the $H_2$ consumption does not occur concurrently with the water production, beginning already at 360 K and maximizing at 470 K. These observations suggest that the interaction with hydrogen at 10 atm occurs at profoundly lower temperatures that, in turn, influences the subsequent reduction of ceria.

10.1002/chem.202005374

Figure 5a shows *in situ* Diffuse Reflectance Infrared Fourier Transform Spectroscopy (DRIFTS) spectra of ceria powders exposed to $H_2$ at various conditions. (Henceforth, the notation $CeO_{2-x}$-X-Y stands for ceria treated in X atm of $H_2$ and temperature Y (in K).) In the $\nu$(OH) region, a vibrational feature at 3666 $cm^{-1}$ emerges upon exposure to 1 atm $H_2$ at 473 K, which grows and shifts to 3655 $cm^{-1}$ at 723 K. In addition, a new broad band centered at 950 $cm^{-1}$ appears. (Weak vibrational features at 860, 1016 and 1044 $cm^{-1}$ in this region arise from adventitious $CO_2$ adsorption.[18]) The spectrum does not change much in 10 atm of $H_2$ at 723 K. Moreover, the observed bands are stable and basically remain after sample cooling to 373 K and subsequent pumping the $H_2$ gas out (Figure S3). Ceria exposed to 10 atm $D_2$ at 723 K revealed a strong OD band at 2691 $cm^{-1}$, which corresponds to the OH counterpart at 3655 $cm^{-1}$ in the $H_2$ experiments, and nicely matches the one observed by IRAS on the ceria films at 500 – 600 K (see Figures 1a and 2a). The 950 $cm^{-1}$ band disappears upon $D_2$ adsorption, indicating that this feature relates to the H-involving vibrations. This band falls in the range of frequencies characteristic for vibrations of bulk Ce-H species.[10,19] Accordingly, Ce-D species would show up at frequencies strongly red-shifted as compared to Ce-H, which is below the cut-off frequency of our setups (both for IRAS studies on thin films and DRIFT studies on powders). Please note in addition, that IRAS spectra on metal supported films obey the well-known metal selection rules[20] and detect only vibrations associated with dipole changes normal to the surface. Therefore, our present results provide first IR-based experimental evidence for the formation of bulk hydride species upon interaction with $H_2$. A relatively large bandwidth indicates the presence of Ce-H in different local environments. In addition to bulk species, the surface Ce-H species was previously observed in oxidized ceria rods exposed to 1 bar $H_2$ at 673 K, which exhibited a vibrational feature at around 500 $cm^{-1}$ in inelastic neutron scattering spectra.[10] Note also indications of Ce-H vibrations in a very recent Raman study of cerium-hydride growth centers on metallic Ce foil.[21]

10.1002/chem.202005374

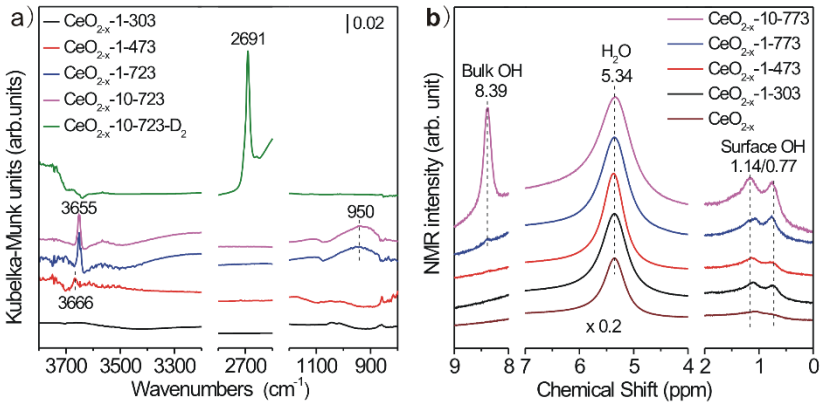


**Figure 5**. A) *In situ* DRIFTS spectra measured for ceria treated in $H_2$ at different conditions and in 10 atm $D_2$ at 723 K. The spectra measured on ceria samples treated in Ar at 723 K and cooled to specified temperatures were used as the references. B) MAS $^1$H NMR spectra measured for ceria treated in $H_2$ at different conditions and then cooled in $H_2$ to room temperature.

Figure 5b displays respective MAS $^1$H NMR spectra of the $H_2$-treated ceria samples. Unfortunately, Ce-H species cannot be detected.[22] Ceria heated at 773 K in He exhibits signals at 1.14/0.77 and 5.34 ppm arising from surface OH groups and adsorbed $H_2O$, respectively.[23] The signals grow with the $H_2$ pressure and temperature. An additional weak feature emerges at 8.39 ppm upon exposure to 1 atm $H_2$ at 773 K and increases significantly upon exposure to 10 atm $H_2$ at 773 K. This feature can be assigned to bulk OH groups in ceria.[23] Therefore, the NMR results provide clear evidence of the increase of the total OH coverage. The OH formation mainly occurs on the surface at temperatures up to 473 K and extends to the bulk region at 773 K. Comparing the evolutions of bulk Ce-H species derived from the *in situ* DRIFTS results and bulk OH group from the NMR results, we infer that the formation of bulk Ce-H species is more favored than that of bulk OH groups in ceria exposed to $H_2$ at 773 K, where bulk reduction occurs and bulk oxygen vacancies form. (The full dataset of DRIFTS and NMR results are shown in Figures S4 and S5).

In order to link these results to the thin film data, the ceria samples were characterized by XPS (Figure 6a and Figures S6a, S7). Based on XPS data, ceria heated to 773 K in He, in order to create oxygen vacancies, exhibits an initial $Ce^{3+}$ concentration of 9.2 % within the near surface region determined by the escape depth of the Ce 3d-electrons (~ 3 nm), henceforth referred to as $Ce^{3+}_{surf}$. Then, the sample was exposed to 1 atm $H_2$ at three different temperatures (303, 473, and 773 K). Consequently, those samples were annealed at the elevated temperatures, up to 773 K, and XPS spectra were recorded. Exposure to 1 atm of $H_2$ at room temperature ($CeO_{2-x}$-1-303) decreases the $Ce^{3+}_{surf}$ concentration, as also observed

10.1002/chem.202005374

above for the films, due to OH and hydride formation and its interconversion. Increase in temperature under the same pressure conditions ($CeO_{2-x}$-1-473, $CeO_{2-x}$-1-773), or in pressure at 773 K ($CeO_{2-x}$-10-773), leads to a smaller effect. Upon vacuum annealing of the samples the amount of $Ce^{3+}_{surf}$ increases due to water desorption and shows the biggest effect for the sample treated at 10 atm.

Now we compare the XPS results with EPR data (spectra are shown in Figures S6b and S8), probing both surface/near surface and bulk species. The relative changes in the $Ce^{3+}$ concentration (henceforth, $Ce^{3+}_{bulk}$), as represented by the EPR intensity normalized to that of pristine ceria (prepared in the same way as the samples for XPS), are shown in Figure 6b. Except the $CeO_{2-x}$-1-473 sample, the $Ce^{3+}_{bulk}$ concentration drops to very low values in $CeO_{2-x}$-1-773 and $CeO_{2-x}$-10-773, as well as for the room temperature sample, clearly indicating bulk hydride formation in these samples. Since EPR probes the entire sample, both surface and bulk, the small amount of $Ce^{3+}$ near the surface (monitored by XPS, Figure 6a) contributes much less to the signal. The obvious increase of $Ce^{3+}$ observed by XPS and EPR on the $CeO_{2-x}$-1-303 sample upon vacuum annealing or purging at 423 K reflects the transformation of surface $Ce^{4+}H^-$ into more stable surface OH, accompanied by the reduction of $Ce^{4+}$ into $Ce^{3+}$, and the decomposition of surface $Ce_{Ov}{}^{4+}H^-$ into hydrogen and $Ce_{Ov}{}^{3+}$.[12] It is interesting to note, that, after He purging at and above 423 K, the EPR data for the $CeO_{2-x}$-1-303 almost match the set of data taken on the $CeO_{2-x}$-1-473 sample. A glance at the water desorption data (Figure S9) tells us that this is due to the onset of water desorption and thus oxygen vacancy formation around 400 K. Both the $Ce^{3+}_{surf}$ and $Ce^{3+}_{bulk}$ concentrations in $CeO_{2-x}$-1-303 and $CeO_{2-x}$-1-473 and the $Ce^{3+}_{surf}$ concentrations in $CeO_{2-x}$-1-773 and $CeO_{2-x}$-10-773 then increase and exceed the initial concentration of $CeO_{2-x}$ upon vacuum annealing or purging at 523 K and above, again, mainly due to the recombinative reaction of surface OH groups to produce water and create $O_v$ and $Ce^{3+}$. However, the $Ce^{3+}_{bulk}$ concentrations in the $CeO_{2-x}$-1-773 and $CeO_{2-x}$-10-773 samples are always lower than the initial concentration, indicating the presence of bulk Ce-H species. They increase upon annealing at 523 - 623 K *via* the reaction $2Ce_{Ov}{}^{4+}H^- \rightarrow H_2(g) + 2Ce_{Ov}{}^{3+}$, but decrease at higher temperatures (773 K), although the $H_2$ production continues (Figure S9). On one hand, this agrees with the DRIFTS results that the $H_2$ productions above 623 K for $CeO_{2-x}$-1-773 and $CeO_{2-x}$-10-773 involve the OH species. On the other hand, this indicates the re-formation of bulk $Ce_{Ov}{}^{4+}H^-$ species most likely by the migration of H atoms in surface OH species to bulk $Ce_{Ov}{}^{3+}$ sites. Similar phenomena were previously observed to occur

10.1002/chem.202005374

on the highly hydrogenated and reduced $TiO_2$ surfaces.[24] These observations demonstrate that the stability of Ce-H species enhances greatly with the $O_v$ concentration in ceria.

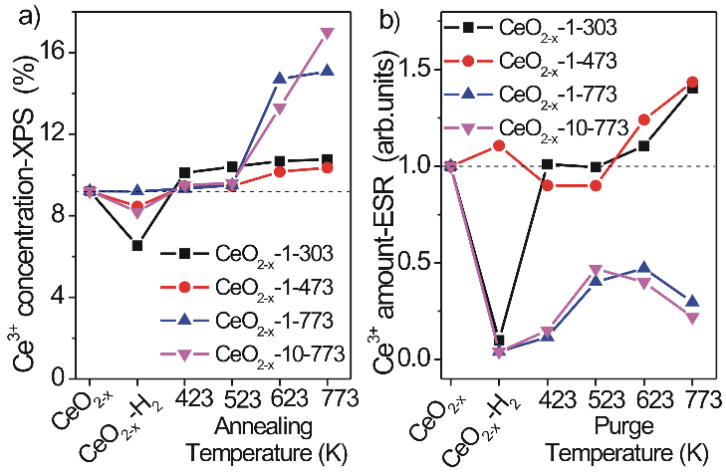


**Figure 6**. a) $Ce^{3+}_{surf}$ concentration derived from XPS and (b) changes in the $Ce^{3+}_{bulk}$ concentration (normalized to pristine ceria) derived from EPR, for ceria samples treated in $H_2$ at different conditions and then cooled in $H_2$ to room temperature followed by vacuum annealing (for 30-60 min) during XPS measurements or purging in He (for 2 hours) during ESR measurements at indicated temperatures.

Summarizing at this point, the variations of $Ce^{3+}_{surf}$ and $Ce^{3+}_{bulk}$ species (determined by XPS and EPR, respectively) indicate relative amounts of $Ce^{3+}$ created by the homolytic dissociation to OH and oxygen vacancy formation reactions (eqs. 1 and 2 in the Introduction), and annihilated by the homolytic dissociation to $Ce_{Ov}{}^{4+}H^-$ (eq. 3), which, together with the formed H species, can be used to deduce which reactions occur upon $H_2$-$CeO_2$ interaction and where. Certainly, the $Ce^{3+}_{surf}$ and $Ce^{3+}_{bulk}$ species overlap in the sub-surface region. Compared to ceria pre-treated at 773 K in He, the $CeO_{2-x}$-1-303 sample contains less $Ce^{3+}_{surf}$ and $Ce^{3+}_{bulk}$, due to the kinetically-favored heterolytic dissociation to OH and $Ce^{4+}H^-$ on the ceria surface (eq. 4) and homolytic dissociation to $Ce_{Ov}{}^{4+}H^-$ at surface oxygen vacancy sites (eq. 3). At 473 and 773 K, $H_2$ undergoes the thermodynamically-favored homolytic dissociation to OH species on the ceria surface, the oxygen vacancy formation reaction, and the homolytic dissociation to $Ce_{Ov}{}^{4+}H^-$ at initially present and newly-formed oxygen vacancies in the sub-surface region, leading to almost unchanged $Ce^{3+}_{surf}$ as initially observed in $CeO_{2-x}$-1-473, $CeO_{2-x}$-1-773 and $CeO_{2-x}$-10-773. The only slightly increased $Ce^{3+}_{bulk}$ concentration observed for $CeO_{2-x}$-1-473 is likely due to either limited creation of bulk oxygen vacancies or the limited diffusivity of hydride filled oxygen vacancies at that temperature. However, $CeO_{2-x}$-1-773 and $CeO_{2-x}$-10-773 with high oxygen vacancy concentrations, arising either from diffusion or creation in the

10.1002/chem.202005374

bulk, exhibit almost no $Ce^{3+}_{bulk}$, indicating the formation of bulk $Ce_{Ov}^{4+}H^{-}$. Those samples also exhibit bulk OH species arising from the homolytic dissociation to OH or the heterolytic dissociation in the bulk.

### *2.3. Theoretical calculations*

To study the relative stabilities of proton ($H^{+}$−O) and hydride ($H^{-}$−Ce) species at $CeO_2$(111) surfaces with different degrees of reduction, we constructed $CeO_2$(111)-*n*$OV_{surf}$ (*n* refers to the number of surface oxygen vacancies ranging from 1 to 4, and *n* = 4 corresponds to a $O_v$ coverage of 0.16 monolayer (ML)) based on the "hydroxyl-vacancy model".[25] Note that for the cases of *n* = 2, 3, and 4, the surface oxygen vacancies form an energetically favorable (linear) surface oxygen vacancy dimer, trimer, and tetramer, respectively (Figure 7a). It can be seen from Figure 8a that, by increasing the concentration of surface oxygen vacancies (*n* = 1 → 4), the adsorption energy (strength) of proton decreases significantly (1.40 → 0.61 eV), which agrees well with the previous theoretical study.[26] In contrast, the adsorption energy of hydride shows an opposite trend. More specifically, the adsorption energy of hydride drastically changes from -0.71 to 0.41 eV, when increasing the concentration of surface oxygen vacancies (*n* = 1 → 4), indicating that surface hydride can be stabilized by oxygen vacancies. Presumably, this is because the electron-donating character of $CeO_2$(111) is enhanced, and, hence, surface hydride gets stabilized. Therefore, it may be expected that surface hydride is more stable than surface hydrogen atom at heavily reduced $CeO_{2-x}$(111) surfaces with *n* > 4, although we were not able to simulate such surfaces due to the high computational cost.

10.1002/chem.202005374

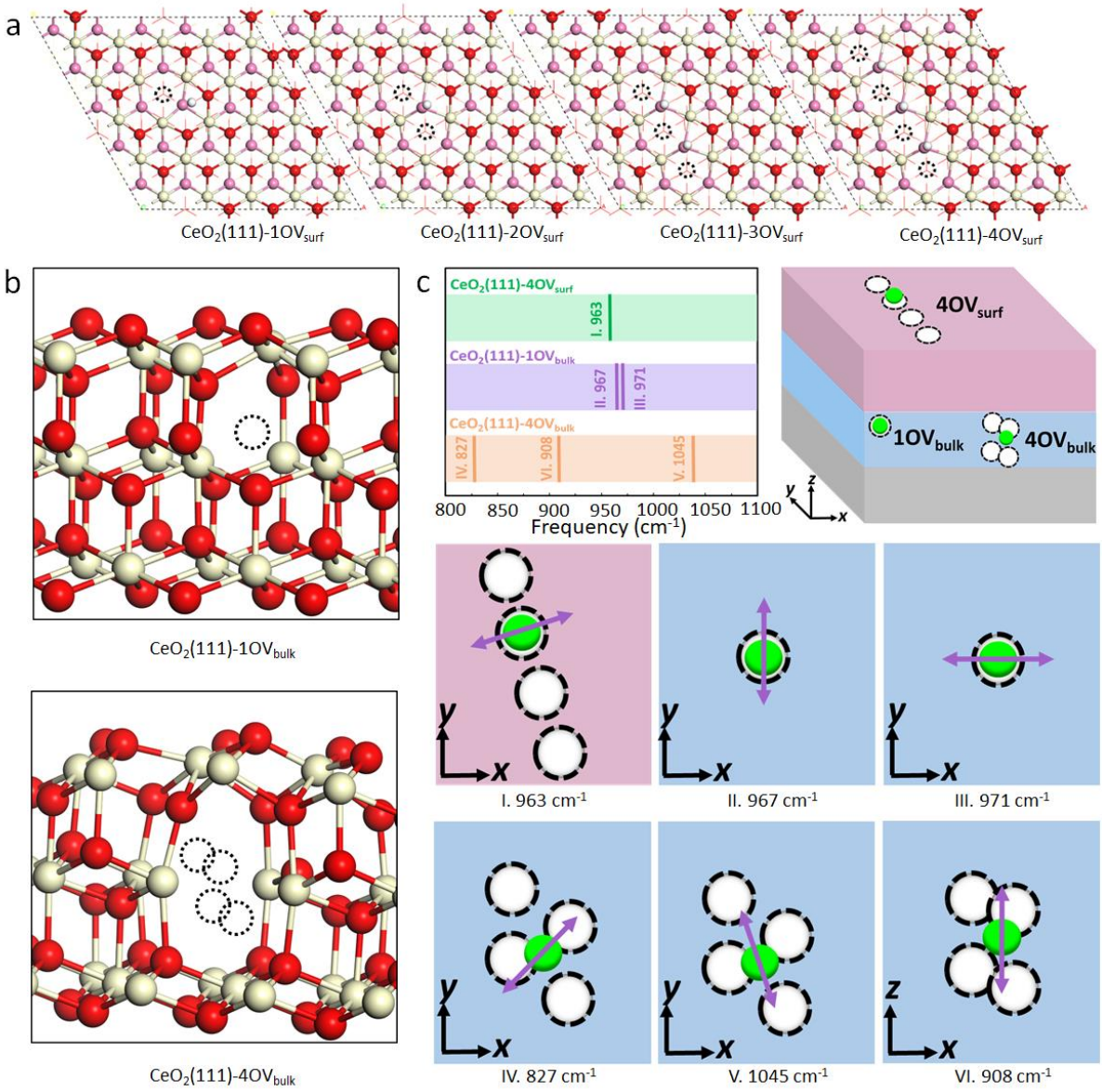


**Figure 7**. (a) Optimized structures (top view) of $CeO_2(111)$-$n$$OV_{surf}$ ($n$ = 1, 2, 3, or 4). Surface cerium, hydrogen, surface oxygen, and subsurface oxygen atoms are represented by gray, white, red, and pink balls, respectively; the bottom two O−Ce−O trilayers are drawn with lines for clarity. (b) Optimized structures (side view) of $CeO_2(111)$-$1OV_{bulk}$ and $CeO_2(111)$-$4OV_{bulk}$. Cerium, hydrogen, and oxygen atoms are in gray, white, and red, respectively. (c) Scaled DFT-calculated vibrational frequencies of surface and bulk hydrides based on the selected models (i.e., $CeO_2(111)$-$4OV_{surf}$, $CeO_2(111)$-$1OV_{bulk}$, and $CeO_2(111)$-$4OV_{bulk}$) and schematic views of the corresponding vibrational modes. The top, middle, and bottom O−Ce−O trilayers of the $CeO_2(111)$ slab are simplified by light red, light blue, and gray sheets, respectively. The purple arrows represent the directions of the vibrations of the hydrides (green balls). In a, b, and c, dashed black circles represent oxygen vacancies.

10.1002/chem.202005374

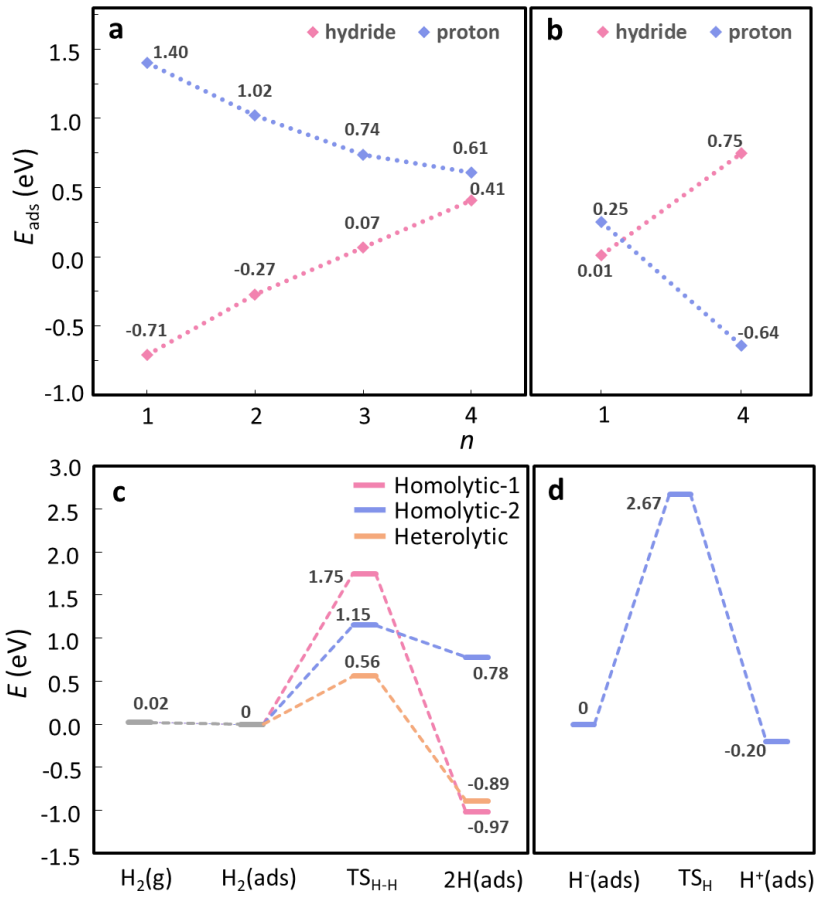


**Figure 8.** Calculated adsorption energies ($E_{ads}$) of hydride and proton as a function of the number of oxygen vacancies based on (a) $CeO_2$(111)-*n*$OV_{surf}$ (*n* = 1, 2, 3, or 4) and (b) $CeO_2$(111)-*n*$OV_{bulk}$ (*n* = 1 or 4). Calculated energy profiles for (c) $H_2$ dissociation on $CeO_2$(111)-4$OV_{surf}$ through the homolytic-1, homolytic-2, and heterolytic pathways and (d) the transformation of surface hydride to surface hydrogen atom on $CeO_2$(111)-4$OV_{surf}$. For c, $H_2$(g), $H_2$(ads), $TS_{H-H}$, 2H(ads) represent respectively the state with gas-phase $H_2$, the surface adsorption state of $H_2$, the transition state of $H_2$ dissociation, and the surface adsorption state of two H (which can be hydride or hydrogen atom). For d, $H^-$(ads), $TS_H$, and $H^+$(ads) represent respectively the surface adsorption state of hydride, the transition state of transformation of hydride to proton, the surface adsorption state of proton. Corresponding structures are shown in Figures S10-S13.

We also evaluated the relative stabilities of hydrogen atom and hydride species in the bulk of ceria by constructing the slab models of $CeO_2$(111) with one and four aggregated oxygen vacancies in the middle O–Ce–O trilayer (denoted as $CeO_2$(111)-1$OV_{bulk}$ and $CeO_2$(111)-4$OV_{bulk}$, respectively, see Figure 7b). Not surprisingly, compared with the surface case, oxygen vacancies in the "bulk" have similar effects on the stabilities of surrounding hydrogen atom and hydride species (see Figure 8b). It is interesting to note that, for the vacancy-rich case of $CeO_2$(111)-4$OV_{bulk}$, hydride is ~1.4 eV more stable than a corresponding

10.1002/chem.202005374

hydrogen atom, suggesting that hydride is the dominant species in the bulk region of heavily reduced ceria. Meanwhile, these results also indicate, that bulk hydride is more stable than surface hydride, whereas a surface hydrogen atom is more stable than a bulk hydrogen atom.

Based on the representative $CeO_2$(111)-4$OV_{surf}$ model, we studied the following three possible dissociation pathways of $H_2$: (i) homolytic dissociation of $H_2$ to two surface hydrogen atoms (denoted as the homolytic-1 pathway); (ii) homolytic dissociation of $H_2$ to two surface hydrides (the homolytic-2 pathway); (iii) heterolytic dissociation of $H_2$ to one surface proton and one surface hydride (the heterolytic pathway). The calculated energy profiles and the relevant structures are presented in Figure 8c and Figure S12, respectively. The three dissociation pathways all start from a weakly adsorbed $H_2$ ($E_{\mathrm{ads}}$ = 0.02 eV) above a Ce atom. We found that the heterolytic pathway gives the lowest activation energy barrier of 0.56 eV, followed by the hemolytic-2 pathway (barrier: 1.15 eV). Although the homolytic-1 pathway is thermodynamically most favorable, it has a highest barrier of 1.75 eV, which is consistent with the previous study.[7b] Therefore, formation of surface hydride through the heterolytic and hemolytic-2 pathways is kinetically favorable on the $CeO_2$(111)-4$OV_{surf}$ surface. We also found that the transformation of surface hydride to surface proton is extremely difficult at $CeO_2$(111)-4$OV_{surf}$ since it needs to overcome a high barrier of 2.67 eV (Figure 8d and Figure S13). Accordingly, hydride is kinetically stable at such surface. Meanwhile, the recombinative desorption of surface hydrides to $H_2$ is most favorable both, thermodynamically and kinetically, among all $H_2$ production pathways from H species. The results based on the $CeO_2$(111)-4$OV_{surf}$ and $CeO_2$(111)-4$OV_{bulk}$ models also suggest that surface hydrides, once formed, can readily diffuse into the bulk region and be stabilized therein at heavily reduced conditions. Therefore, the DFT results fully agree with the above experimental observations for $H_2$-$CeO_{2-x}$ powder systems.

The scaled DFT-calculated vibrational frequencies of surface and bulk hydrides based on the selected models (*i.e.*, $CeO_2$(111)-4$OV_{surf}$, $CeO_2$(111)-1$OV_{bulk}$, and $CeO_2$(111)-4$OV_{bulk}$) are summarized in Table S1. The vibrations of bulk hydride depend strongly on the configuration of oxygen vacancies, but they cover the experimentally observed broad vibrational band centered at 950 $cm^{-1}$ (Figure 7c). For surface hydride, the vibration at 963 $cm^{-1}$ (Figure 7c) exhibits a dipole moment parallel to the surface, which rationalizes its absence in IRAS experiments with $CeO_{2-x}$(111) thin film due to the well-known metal surface selection rule applied in IRAS. [20]

10.1002/chem.202005374

## 3. Summary

Our combined experimental and computational results provide a comprehensive picture of the $H_2$-ceria interaction and highlight the vital role of oxygen vacancies in this process as well as the important interplay between surface and bulk. On a stoichiometric $CeO_2$ surface, $H_2$ only dissociates to form surface hydroxyls at elevated temperatures. On reduced $CeO_{2-x}$, hydroxyls and hydrides are formed on the surface and in the bulk, depending on $O_v$ concentration and location. The general trends are that hydroxyl is destabilized as the $O_v$ coverage increases, whereas hydride is stabilized, and that surface hydroxyl is more stable than bulk hydroxyl, whereas bulk hydride is more stable than surface hydride. The surface hydride formation is the kinetically-favorable process at relatively low temperatures, and the resulting surface hydride can easily diffuse into the bulk region and get stabilized therein. At higher temperatures, surface hydroxyls can react to produce water and create additional oxygen vacancies, which in turn control the $H_2$-ceria interaction.

The results demonstrate the facile formation of hydride ($Ce_{Ov}^{4+}H^-$) at the $Ce_{Ov}^{3+}$ site, leading to the oxidation of $Ce_{Ov}^{3+}$. $Ce^{3+}$ sites associated with oxygen vacancies play an important role in determining the $CeO_{2-x}$ reactivity, therefore, their annihilation *via* the $Ce_{Ov}^{4+}H^-$ formation will affect the $CeO_{2-x}$ reactivity. The results also demonstrate the hydride formation at the *in situ* created oxygen vacancy sites of ceria during the reduction process, suggesting that the ceria reduction by $H_2$ should follow the reaction equation $CeO_2 + (x+y)H_2 \rightarrow CeO_{2-x} + xH_2O + 2yCe_{Ov}^{4+}H^- + (x-y)O_v$ rather than $CeO_2 + xH_2 \rightarrow CeO_{2-x} + xH_2O + xO_v$.

We believe that our results showing the diversity of reaction pathways taking place upon interaction of $H_2$ with ceria will aid in full understanding of the reactivity of ceria-based catalysts in a hydrogen-rich atmosphere.

**Acknowledgements**

This work is financially supported by National Key R & D Program of MOST (2017YFB0602205), the DFG-NSFC joint project (Nos. FR554/18-1 and 21761132005), the National Natural Science Foundation of China (91945301, 21525313, 91745202, U1930203, 21825301), the Chinese Academy of Sciences, and the Changjiang Scholars Program of Ministry of Education of China. HJF thanks Fonds der Chemischen Industrie. JQZ thanks the AvH Foundation for a fellowship.

## References


[1] a) Z. Paál, P. G. Menon, *Hydrogen Effects in Catalysis: Fundamentals and Practical Applications*, Marcel Dekker Inc., New York, **1988**; b) T. Norby, M. Widerøe, R. Glöckner, Y. Larring, *J. Chem. Soc. Dalton Trans.* **2004**, 3012-3018; c) R. Más-Balleste, A. Lledos, In *Comprehensive Inorganic Chemistry II: From Elements to Applications*, *Vol. 9* (Eds.: J. Reedijk, K. Poeppelmeier), Elsevier, Oxford, **2013**, p 727.

[2] a) V. E. Henrich, P. A. Cox, *The Surface Science of Metal Oxides*, Cambridge University Press, Cambridge, **1994**; b) J. L. G. Fierro, *Metal Oxides: Chemistry and Applications*, CRC Press, Boca Raton, **2006**; c) C. Copéret, D. P. Estes, K. Larmier, K. Searles, *Chem. Rev.* **2016**, *116*, 8463–8505.

[3] a) G. Vilé, B. Bridier, J. Wichert, J. Pérez-Ramírez, *Angew. Chem. Int. Ed.* **2012**, *51*, 8620-8623; b) J. Carrasco, G. Vilé, D. Fernández-Torre, R. Pérez, J. Pérez-Ramírez, M. V. Ganduglia-Pirovano, *J. Phys. Chem. C* **2014**, *118*, 5352-5360; c) G. Vilé, S. Colussi, F. Krumeich, A. Trovarelli, J. Pérez-Ramírez, *Angew. Chem. Int. Ed.* **2014**, *53*, 12069-12072; d) G. Vilé, P. Dähler, J. Vecchietti, M. Baltanás, S. Collins, M. Calatayud, A. Bonivardi, J. Pérez-Ramírez, *J. Catal.* **2015**, *324*, 69-78; e) T. Cao, R. You, X. Zhang, S. Chen, D. Li, Z. Zhang, W. Huang, *Phys. Chem. Chem. Phys.* **2018**, *20*, 9659-9670; f) T. Cao, R. You, Z. Li, X. Zhang, D. Li, S. Chen, Z. Zhang, W. Huang, *Appl. Surf. Sci.* **2020**, *501*, 144120; g) J. Moon, Y. Cheng, L. L. Daemen, M. Li, F. Polo-Garzon, A. J. Ramirez-Cuesta, Z. Wu, *ACS Catal.* **2020**, *10*, 5278−5287.

[4] C. Binet, M. Daturi, J.-C. Lavalley, *Catal. Today* **1999**, *50*, 207−225.

[5] K. Sohlberg, S. T. Pantelides, S. J. Pennycook, *J. Am. Chem. Soc.* **2001**, *123*, 6609−6611.

[6] a) D. Fernández-Torre, J. Carrasco, M. V. Ganduglia-Pirovano, R. Pérez, *J. Chem. Phys.* **2014**, *141*, 014703; b) F. R. Negreiros, M. F. Camellone, S. Fabris, *J. Phys. Chem. C* **2015**, *119*, 21567-21573; c) M. García-Melchor, N. López, *J. Phys. Chem. C* **2014**, *118*, 10921-10926.

[7] a) Z.-Q. Huang, L.-P. Liu, S. Qi, S. Zhang, Y. Qu, C.-R. Chang, *ACS Catal.* **2017**, *8*, 546-554; b) C. Riley, S. Zhou, D. Kunwar, A. De La Riva, E. Peterson, R. Payne, L. Gao, S. Lin, H. Guo, A. Datye, *J. Am. Chem. Soc.* **2018**, *140*, 12964-12973.

[8] a) B. Chen, Y. Ma, L. Ding, L. Xu, Z. Wu, Q. Yuan, W. Huang, *J. Phys. Chem. C* **2013**, *117*, 5800-5810; b) Y. Gao, R. Li, S. Chen, L. Luo, T. Cao, W. Huang, *Phys. Chem. Chem. Phys.* **2015**, *17*, 31862-31871.

[9] M. Nolan, J. E. Fearon, G. W.Watson, *Solid State Ionics* **2006**, *177*, 3069-3074.

[10] Z. Wu, Y. Cheng, F. Tao, L. Daemen, G. S. Foo, L. Nguyen, X. Zhang, A. Beste, A. J. Ramirez-Cuesta, *J. Am. Chem. Soc.* **2017**, *139*, 9721-9727.

[11] K. Werner, X. Weng, F. Calaza, M. Sterrer, T. Kropp, J. Paier, J. Sauer, M. Wilde, K. Fukutani, S. Shaikhutdinov, *J. Am. Chem. Soc.* **2017**, *139*, 17608-17616.

[12] Z. Li, K. Werner, K. Qian, R. You, A. Plucienik, A. Jia, L. Wu, L. Zhang, H. Pan, H. Kuhlenbeck, S. Shaikhutdinov, W. Huang, H.-J. Freund, *Angew. Chem. Int. Ed.* **2019**, *58*, 14686-14693.

[13] D. Schweke, L. Shelly, R. Ben David, A. Danon, N. Kostirya, S. Hayun, *J. Phys. Chem. C* **2020**, *124*, 6180−6187.

[14] a) S. Chen, F. Xiong, W. Huang, *Surf. Sci. Rep.* **2019**, *74*, 100471; b) H.-J. Freund, M. Heyde, H. Kuhlenbeck, N. Nilius, T. Risse, Th. Schmidt, S. Shaikhutdinov, M. Sterrer, *Sci. China. Chem.* **2020**, *63*, 426-447.

[15] D.R. Mullins, *Surf. Sci. Rep.* **2015**, *70*, 42-85.

10.1002/chem.202005374

[16] a) A. Badri, C. Binet, J.-C. Lavalley, *J. Chem. Soc. Faraday Trans.* **1996**, *92*, 4669-4673; b) S. Bernal, J. J. Calvino, G. A. Cifredo, J. M. Gatica, J. A. P. Omil, J. M. Pintado, *J. Chem. Soc. Faraday Trans.* **1993**, *89*, 3499-3505.

[17] E. Aneggi, D. Wiater, C. de Leitenburg, J. Llorca, A. Trovarelli, *ACS Catal.* **2014**, *4*, 172-181.

[18] A. Trovarelli, *Catal. Rev.* **1996,** *38*, 439-520.

[19] a) A. Fujimori, M. Ishii, N. Tsuda, *Phys. Status Solidi B* **1980**, *99*, 673-681; b) O. Matz, M. Calatayud, *ACS Omega* **2018**, *3*, 16063-16073.

[20] S. A. Francis, A. H. Ellison, *J. Opt. Soc. Am.* **1959,** *49*, 131-138.

[21] T. Livneh, D. Avisar. *J. Phys. Chem. C*, in press.

[22] a) C. Lundin, *Rare Earth Research*. *Vol. 1*, CRC Press, **1962**; b) L. Maron, E. L. Werkema, L. Perrin, O. Eisenstein, R. A. Andersen, *J. Am. Chem. Soc.* **2005**, *127*, 279-292.

[23] L. Gill, A. Beste, B. Chen, M. Li, A. K. Mann, S. H. Overbury, E. W. Hagaman, *J. Phys. Chem. C* **2017**, *121*, 7450-7465.

[24] a) Z. Wu, F. Xiong, Z. Wang, W. Huang, *Chin. Chem. Lett.* **2018**, *29*, 752-756; b) J. Tao, Q. Cuan, X.-Q. Gong, M. Batzill, *J. Phys. Chem. C* **2012**, *116*, 20438-20446; 45c) X. L. Yin, M. Calatayud, H. Qiu, Y. Wang, A. Birkner, C. Minot, C. Wöll, *ChemPhysChem* **2008**, *9*, 253-256

[25] X.-P. Wu, X.-Q. Gong, *Phys. Rev. Lett.* **2016**, *116*, 086102.

[26] X.-P. Wu, X.-Q. Gong, G. Lu, *Phys. Chem. Chem. Phys.* **2015**, *17*, 3544-3549.